

## CHANGES IN THE OPTICAL REMNANT OF KEPLER'S SUPERNOVA DURING THE PERIOD 1942–1989<sup>1</sup>

RINO BANDIERA

Osservatorio Astrofisico di Arcetri, Largo Enrico Fermi, 5, 50125 Firenze, Italy

AND

SIDNEY VAN DEN BERGH<sup>2</sup>

Dominion Astrophysical Observatory, National Research Council of Canada, 5071 West Saanich Road, Victoria, BC, Canada V8X 4M6

Received 1990 October 8; accepted 1990 December 4

### ABSTRACT

Images of the optical nebulosity associated with Kepler's supernova = 3C 358 = G4.5 + 6.8 have been obtained at the Mount Wilson Observatory in 1941–1943, at the Palomar Observatory in 1950–1983, and on La Silla in 1989. These data have been used to study the luminosity evolution of individual knots and the expansion and translation of the optical remnant of Kepler's supernova of 1604. From a study of the motions of 50 long-lived knots we find  $\langle \mu_x \rangle = -0''.623 \pm 0''.045$  century<sup>-1</sup>,  $\langle \mu_y \rangle = 0''.484 \pm 0''.049$  century<sup>-1</sup> and an expansion time scale of  $32,000 \pm 12,000$  yr. For an assumed distance of 4.5 kpc the centroid of the nebulosity has a tangential velocity of  $117 \pm 10$  km s<sup>-1</sup> to the W and  $105 \pm 11$  km s<sup>-1</sup> to the N. By combining astrometric and spectroscopic information, a space velocity of  $278 \pm 12$  km s<sup>-1</sup> is estimated. This indicates that the progenitor of SN 1604 was a high-velocity object. It could have been either a Population II star or a massive high-velocity runaway star.

Comparison of old and new images indicates that most new knots occur along the outer part of the northern rim of the supernova remnant (SNR). Recently some knots have also appeared near the center of the remnant, to the south of those already existing. The evolutionary time scales of knots in Kepler's SNR are similar to those of quasi-stationary flocculi in Cassiopeia A, but considerably longer than those of fast-moving knots in Cas A.

*Subject headings:* nebulae: individual (Kepler's supernova) — nebulae: internal motions — nebulae: supernova remnants

### 1. INTRODUCTION

The optical remnant of Kepler's supernova of 1604 was discovered by Baade (1943). Subsequent studies of the morphology of this object are by van den Bergh, Marscher, & Terzian (1973), van den Bergh & Kamper (1977), and by D'Odorico et al. (1986). In addition to emission from bright knots, Fesen et al. (1989) have recently discovered the presence of faint diffuse Balmer-dominated emission (often referred to as "nonradiative" emission) that is associated with the remnant's high-velocity shock. The positions of the strongest non-radiative Balmer emission filaments correspond to the highest surface brightness regions of the radio shell of 3C 358 = G4.5 + 6.8 (Dickel et al. 1988). Because of its large distance from the Galactic plane ( $z = 530$  pc for a distance of 4.5 kpc; see § 3.5) the progenitor of SN 1604 has usually been regarded as a supernova of Type Ia. Recently Bandiera (1987) has, however, given arguments suggesting that Kepler's supernova might, in fact, have been produced by a massive runaway star.

Kepler's supernova remnant is located in a rich star field ( $l = 4^\circ 5$ ,  $b = +6^\circ 8$ ) that is projected on the central bulge of the Galaxy. Crowding therefore makes it very difficult to study the structure and evolution of the optical nebulosity. Since most field stars in this region are reddened red giants (van den Bergh & Kamper 1977) such crowding effects are particularly severe in red exposures that exhibit H $\alpha$  + [N II] or [S II] emission. In the present investigation we shall show that the effects of such

crowding can be greatly reduced by digitally subtracting the continuum from images that are dominated by line emission.

This paper is organized as follows. In § 2 we present the available data consisting of recent CCD frames and various photographic plates obtained during the period 1941–1983. We also describe the data reduction procedures in detail. High-quality CCD observations through broad and narrow bands were used to subtract stellar images from the old photographic plates of this crowded field. In § 3 we give a qualitative discussion of the evolution of the nebulosity. In this section we also present a catalog of positions and proper motions for 50 nebular knots. These data are then used to determine both the expansion and the translation of the remnant of Kepler's supernova. Furthermore we have produced a catalog of the light curves of knots for the last half-century. Finally we discuss presently available evidence on the distance to, and luminosity of, SN 1604.

### 2. OBSERVATIONAL DATA

The available material consists of old photographic plates and recent CCD frames. In the description of this material we shall not follow the chronological order of the observations, but rather the order in which data reduction proceeded. In short, we first reduced CCD frames, in order to get clean images of the nebular emission, as well as of the continuum emission by stars. The continuum frames were then used to produce a reference image of the star field, which was needed for stellar subtraction on the digitized photographic plates.

<sup>1</sup> Partly based on observations made at ESO La Silla Observatory.

<sup>2</sup> Guest Observer Palomar Observatory.

TABLE 1  
INFORMATION ON FILTERS USED FOR CCD  
OBSERVATIONS

Filter	$\lambda$ (max) (Å)	$T$ (max) (%)	FWHM (Å)
H $\alpha$ + [N II] .....	6547	87	82
Continuum .....	6642	83	80
[S II] .....	6742	89	85
Bessell <i>V</i> .....	5253	88	1167
Bessell <i>R</i> .....	6005	85	1640
Gunn <i>r</i> .....	6866	84	1113
Gunn <i>i</i> .....	8194	86	1386

### 2.1. CCD Observations

The CCD observations employed in the present investigation were carried out in 1989 by Bandiera with the 1.5 m Danish telescope on La Silla. Similar observations, carried out almost simultaneously with the 3.6 m CFH telescope in Hawaii by Pritchett and van den Bergh, were used for qualitative checks on the present work. The detector used for the La Silla observations was the "double density" RCA CCD No. 15, which has  $1024 \times 640$  pixels of  $15 \times 15 \mu\text{m}$ . These dimensions correspond to  $0''.232 \times 0''.232$  on the sky. For our La Silla observations we used four different broad-band filters plus three narrow-band ones. Details on each of these filters are given in Table 1. Exposure times were 10 minutes for all broad-band observations and 15 minutes for all narrow-band observations. In order to correct for cosmic rays and CCD defects, multiple exposures with three different pointings, each separated on the sky by 4 pixels, were obtained through each filter.

Three nights of observing (1989 June 29–July 2) were scheduled for the present program. Only during the last night of our run did we encounter reasonably good ( $1''.0$ – $1''.5$ ) seeing. Most of the material actually used in the present investigation was obtained during this last night of observations.

### 2.2. Reduction of CCD Observations

All data reduction was carried out using the portable version of MIDAS, the data analysis system developed by ESO, installed on a Sun 4 workstation. Our reduction procedures were intended to stress the production of images that were as clean and sharp as possible and to deemphasize detection of very faint structures. Unfortunately CCD No. 15 exhibits a large number of cosmetic defects that include both hot spots and cold columns. Standard flat-fielding techniques did not completely remove all of the problems resulting from such defects of the chip. We therefore synthesized from each image a pattern of cold columns which was then subtracted from the image itself. By means of this procedure we were able to obtain a smooth background but lost information on the actual background level.

A hotspot was replaced by the median of neighboring pixels; but, in order to avoid an excess of smoothing (which could degrade the resolution), we applied this substitution only to those hotspots that differed from their surroundings by more than 50%. Residual defects and cosmic rays were eliminated later on, when final images in each color were obtained by forming the median of the three best frames, with different pointings, in that color. Before merging frames, they were aligned using 10 stars in each field. Typical residuals in star positions after such mergers were  $\sim 0.1$  pixel. Furthermore, the

two images of highest resolution were degraded by Gaussian smoothing until their pointspread functions were identical to that on the poorest resolution member of the triplet. After this treatment the resolutions of the three images did not differ from each other by more than 1%. Once the resolutions of each of the three images had been made similar to each other the relative intensity scale of each pair of frames was obtained by a linear regression between the intensities of corresponding pixels. In this way the intensity scales on different frames could be made to agree with each other to better than 0.5%. Needless to say, these averaging techniques will only result in lowering the noise level if the images that are being combined are already very similar to each other. Because our pixel size was very much smaller than the size of the seeing disk manipulations such as filtering, Gaussian fitting to star profiles, and image convolution did not result in significant image degradation.

The reduction procedures described above were applied to images obtained through all seven filters used during our CCD observations. After further point spread function equalization, scaled continuum images were subtracted from the line images in H $\alpha$  + [N II] and [S II]. Furthermore small-scale corrections had to be applied to correct for slight ( $< 0.07\%$ ) differences in the effective focal lengths for observations through different filters. After cleaning by stellar subtraction the FWHM "seeing" in the H $\alpha$  + [N II] and [S II] images was  $\sim 1''.4$ . In the subsequent discussion, in which the H $\alpha$  + [N II] CCD frame will be compared with older photographic images, the 1989 CCD frame will be labeled "89JUL."

The next step in the reduction consisted in subtraction of the nebular contribution from the broad-band CCD frames, in order to obtain a frame showing only the stellar emission. After experimentation with various combinations of H $\alpha$  + [N II] and [S II] images (in order to simulate the overall effect of nebular emission in the broad-band frames) we finally decided to subtract just the H $\alpha$  + [N II] line image. In those cases in which the H $\alpha$  + [N II] image had worse "seeing" than that of the broad-band frame, we did *not* broaden the latter before line subtraction. Since knots are already somewhat resolved, their contribution was well subtracted, without degrading the final resolution too much.

As will be described in more detail later on, a reference stellar image was used for stellar subtraction from individual linearized and digitized photographic images. This reference image reproduces the spectral response of the old photographic plates reasonably well. We found that a quite satisfactory fit to the spectral response of the available plates could be obtained rather easily from a linear combination of various broad-band CCD frames. In our experience an accurate fit to the spectral response of photographic plates was less critical than equalization of seeing and correct determination of the characteristic curve for each photographic plate. The two filters whose effective spectral ranges are most similar to those of our photographic plates were Bessell *R* and Gunn *r* (Bessell 1983; Thuan & Gunn 1976). In order to synthesize the continuum image needed for stellar subtraction from photographic plates we used the Bessell *R* star image directly, since it had better resolution ( $\sim 1''.3$ ) than our Gunn *r* frame.

### 2.3. Photographic Material

For the present investigation we studied 19 photographic plates obtained between 1941 and 1983. A journal of observations for these data is presented in Table 2. It is a source of real

TABLE 2  
JOURNAL OF PHOTOGRAPHIC OBSERVATIONS

Telescope	Date (UT)	Plate Number <sup>a</sup>	Emulsion	Filter	Exposure Time (minute)	Label
2.5 m Hooker	1941 Jun 24	B1180B	103E	RG2	185	
2.5 m Hooker	1942 May 19	B1244B	103E	RG2	205	42MAY
2.5 m Hooker	1942 Jun 14	B1261B	103E	RG2	70	42JUN
2.5 m Hooker	1943 Jul 4	B1390B	103E	RG2	42	
5.0 m Hale	1950 May 23	PH72B	103aE	RG2	120	50MAY
5.0 m Hale	1950 Jul 19	PH163B	103aE	RG2	98	50JUL
5.0 m Hale	1951 Jul 8	PH432B	103U	GG11	120	
5.0 m Hale	1955 May 26	PH1216B	103aE	RG2	100	
5.0 m Hale	1958 May 16	PH1907B	103aF	RG2	110	58MAYa
5.0 m Hale	1958 May 17	PH1915B	103aF	RG2	90	58MAYb
5.0 m Hale	1969 Jun 16	PH5360vB	103aE	RG2	90	
5.0 m Hale	1970 Sep 1	PH5641vB	103aF	RG2	60	
5.0 m Hale	1971 Aug 25	PH5904A	103aF	RG2	40	71AUG
5.0 m Hale	1973 Aug 2	PH6569vB	098	RG2	53	73AUG
5.0 m Hale	1974 Aug 16	PH6917vB	103aE	RG2	83	74AUG
5.0 m Hale	1975 Jul 17	PH7068vB	103aE	H $\alpha$	90	
5.0 m Hale	1975 Jul 18	PH7074vB	103aE	H $\alpha$	120	
5.0 m Hale	1980 Jul 15	PH7774vB	098	RG645	60	80JUL
5.0 m Hale	1983 Jul 14	PH8200vB	098	H $\alpha$	165	83JUL

<sup>a</sup> A, Arp; B, Baade; vB, van den Bergh

regret that the fine 3.5 hr broad-band red exposure made on 1942 June 9, which is reproduced in Baade (1943), is presently missing from the files of the Carnegie Observatories. This plate appears to have been of higher quality than any of the old Mount Wilson plates available to us. Some plates were not used if better material of comparable age was available. Only the 11 best images (taken between 1942 and 1983 and labeled in Table 2 as 42MAY, etc.) have been used in the present study.

#### 2.4. Reduction of Photographic Material

We started by correcting for image distortions on each plate. To do this we searched for stellar objects and established correspondences between them and stars recognized as such in the reference CCD image (Bessell *R* with nebular emission subtracted). The star search was carried out with the INVENTORY routine (West & Kruszewski 1982) implemented in the MIDAS system, which automatically searches for stellar objects. INVENTORY provides not only the positions of the selected objects, but also a list of information such as image intensity, size, etc. Typically we found  $\sim 300$  correspondences between stellar objects on each plate and on the CCD reference frame.

We then discarded stars which were very faint (since their positions cannot be determined very accurately) as well as those which were too bright (these are usually relatively nearby stars, and sometimes exhibit considerable proper motions). The remaining stars (usually  $\geq 100$ ) were then used to fit the plate distortions by a fourth-degree polynomial. Typical residuals from such a fit were  $\sim 0''.2$ .

The next step was to correct for the nonlinearity of the response curve of each photographic plate by direct comparison with stars on our CCD image. In principle, this procedure can only be carried out accurately if the point spread function of a plate is very similar to that in our reference image. An approximate solution to this problem was, however, obtained by a comparison of the intensities of the stellar images that INVENTORY found in common between each photographic plate and the reference image. We then plotted intensities in the

reference image versus those obtained from the photographic plate. After discarding a few deviant points the observed relation was fitted by a fourth-order polynomial with a null constant term. This curve was then used to linearize the characteristic curve of the photographic plate. Images of the brightest stars exhibited considerable scatter and had to be discarded. Therefore it was not possible to calibrate the brightest part of the characteristic curve accurately, and the linearization of the plate sensitivity (a necessary correction before stellar subtraction) was not perfect. As a result considerable positive and negative residuals remain at the positions of the brightest stars in "cleaned" images. The fact that the images of bright stars cannot be completely removed by subtraction detracts from the aesthetic quality of the cleaned images but does not greatly affect their information content. For fainter stars, of which there are many more, a good fit was obtained to the characteristic curve. As a result such faint stars are almost completely removed on cleaned images.

The principal steps of the data reduction, for the region containing the brightest knots, are summarized in Figure 1. This figure should be read from left to right, top first, bottom last. We started by obtaining both a broad-band red ("Bessell *R*") frame with a spectral response similar to those of the photographic plates, and a narrow-band image centered on H $\alpha$  + [N II] ("H $\alpha$  + [N II]"), and finally a third image in a narrow-band continuum filter near H $\alpha$  ("Cont. near H $\alpha$ "). By subtracting the continuum from the H $\alpha$  + [N II] filter, we extracted the pure line emission ("H $\alpha$  + [N II] line") image. This was then used to eliminate the line component from the Bessell *R* image, and to synthesize an image of the pure continuum ("— line"). By subtracting the stellar continuum from a broad-band red exposure obtained in 1950 May ("Old plate 1950") we obtained an image of the nebulosity ("Stars Subtr."). Once the stars are reasonably well subtracted, one can enhance ("Enhanced") the contrast and study faint nebulosity.

As an example of the reduction procedure described above, Figure 2a and Figure 2b show an image obtained in 1950 July before and after subtraction of the stellar images, respectively.

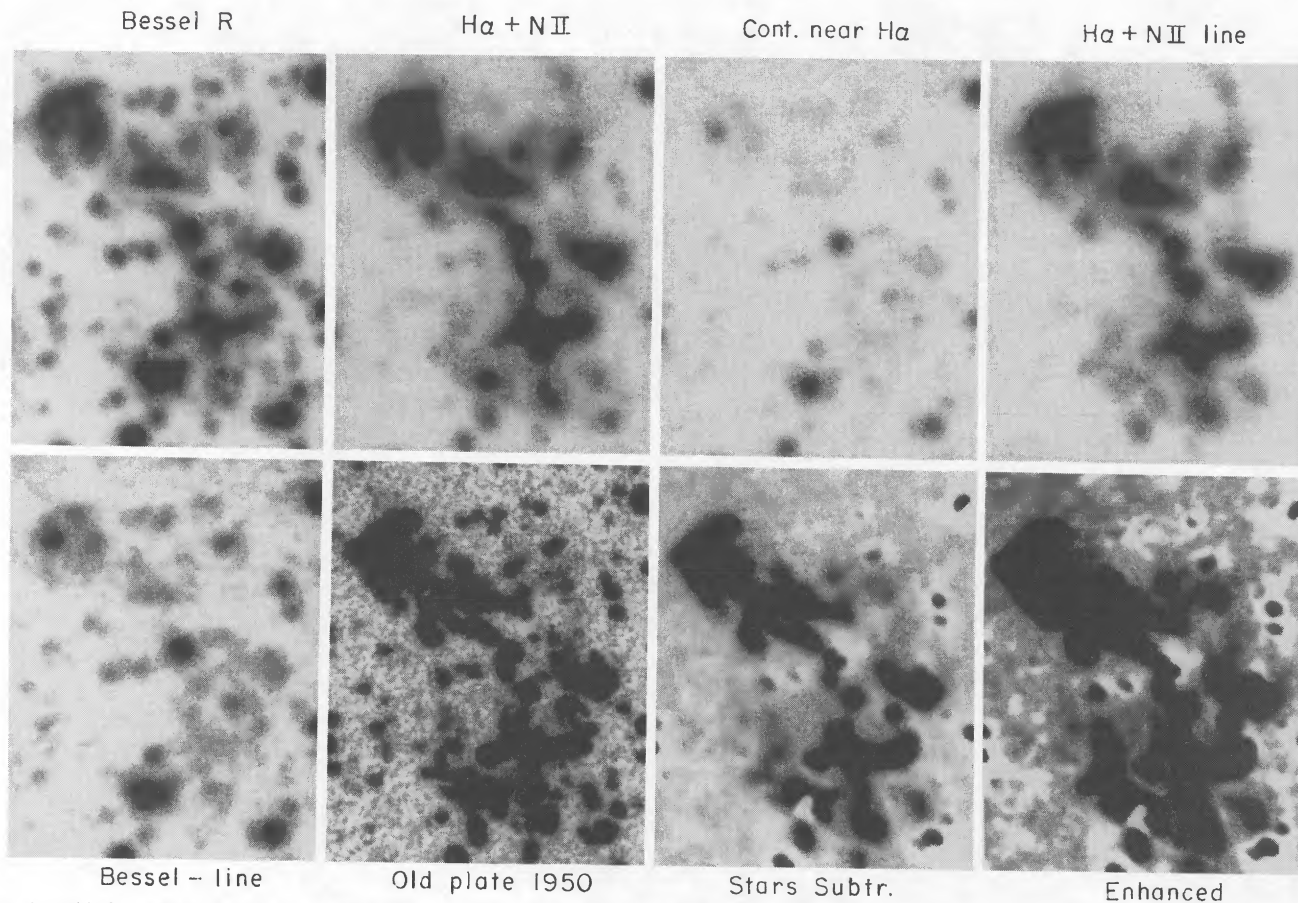


FIG. 1.—This figure illustrates various steps in the reduction and cleaning of CCD frames (*top*) and photographic plates (*bottom*) of the brightest emission region in the remnant of Kepler's supernova.

### 3. DISCUSSION

#### 3.1. Evolution of the Optical Knots

The radio remnant of Kepler's supernova (Dickel et al. 1988) is an almost spherical shell with a radius of  $\sim 100''$ . Its optical emission (e.g., D'Odorico et al. 1986; Fesen et al. 1989) is,

however, restricted to a number of bright patches that are mainly located along the northern and eastern parts of the radio shell, as well as near its center. For the subsequent discussion we have selected nine windows (see Fig. 3) which contain most of the optical knots. Some optical emission falls outside these windows (e.g., above region No. 1, above region

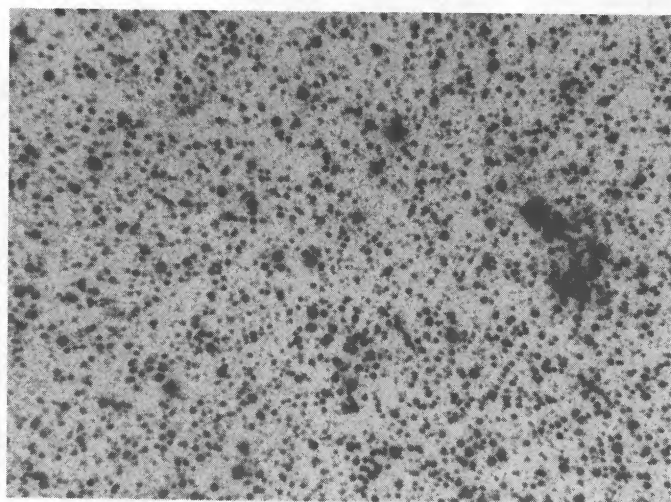


FIG. 2a

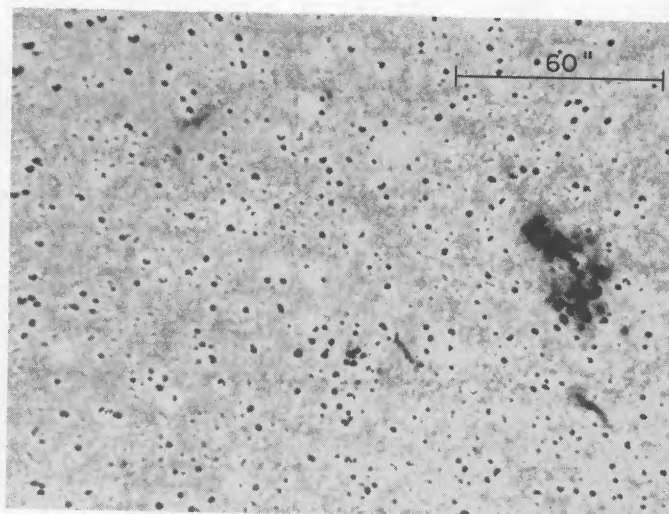


FIG. 2b

FIG. 2.—(a) Broad-band red image of Kepler's SNR. (b) Same as (a) but after "CLEANING" by subtraction of stellar broad-band image.

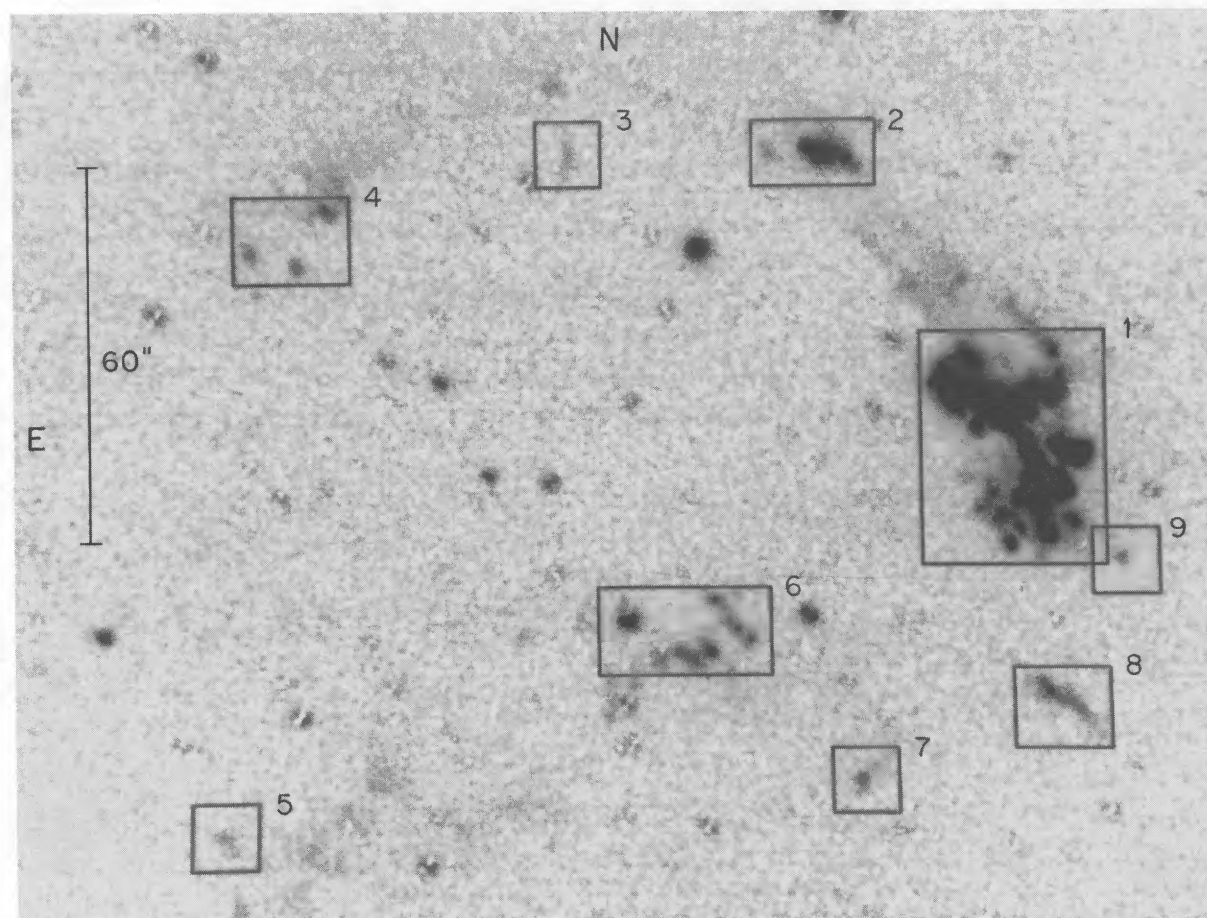


FIG. 3.—CCD image of  $H\alpha + [N II]$  emission of Kepler's SNR showing locations of nine windows that contain most of the emission nebulosity

No. 4 and near region No. 5). Most of the emission outside the windows consists of diffuse nebulosity or of young knots that cannot be seen on older plates. The main purpose of the present investigation is to trace the motions and brightness evolution of individual knots. We shall therefore only consider those knots that are clearly seen on many plates, i.e., mainly bright and rather old knots.

In the next set of figures we present a chronological sequence of images for each of the nine windows. All images are shown to the same angular scale, which is indicated in Figure 2*b* and in Figure 3, which is  $150''$  long in the N–S direction and extends  $200''$  in the E–W direction. In order to facilitate inter-comparisons between individual images within a single window, the various gray levels in each set of images were equalized. In each sequence of images of a particular window the image in the upper left-hand corner shows our identification numbers (see Table 3) for individual knots, while the frame next to it (marked “Orig.”) shows a direct print from Baade's broad-band red plate of 1950 May. The frame marked “Stars” shows the stellar background that was subtracted from all the other frames in each figure. The remaining frames are identified by labels (see Table 2) which refer to the year and month on which they were obtained. The 2.5 m Mount Wilson images obtained in 1942 May and June are, unfortunately, of lower quality than all of the frames obtained subsequently. Note that there are a few bright stars (four in window No. 1, one in window

No. 2, and one in window No. 4) which are poorly subtracted in most or all of our frames.

Figures 4*a*–4*b* show the evolution of the brightest knots in window No. 1, whereas Figures 5*a*–5*b* show the evolution of the fainter features in this area. During the period 1942–1989 a new knot (No. 10) formed on the outside of the main optical shell, while some features (Nos. 15, 29, and probably some diffuse emission NE of No. 26) located on the side of the shell faded. Knots No. 18 and No. 20 also appear to have brightened during recent decades. Figure 6 shows that knots 36 and 37 have become visible during the last two decades. A number of fainter features are of even more recent origin. A common characteristic of those knots is their short turn-on time of only a few years.

Figure 7 of window No. 3 shows no significant brightness evolution of the single wisp of nebulosity (No. 47) in this field. In window No. 4 (Fig. 8) a bright knot has recently appeared near the eastern edge of the frame. This feature has not been included in the catalog because it was not clearly visible prior to 1983 July. This means that its turn-on time scale was only a few years. A rather faint knot, No. 50, is located in window No. 5 (Fig. 9), in a region exhibiting some extended emission. Window No. 6 (see Fig. 10), which is located near the center of the remnant, contains a number of knots; some of which appear to form an extended filament. The other knots (in particular Nos. 42 and 43) are of recent origin and are presently

TABLE 3  
POSITIONS AND PROPER MOTIONS OF KNOTS

N.	Obs.	$\Delta x$	$\Delta y$	$\alpha(1950)$	$\delta(1950)$	DBDF	vdBK	$\mu_x$	$\mu_y$
1	11	-91.5	19.5	17 27 35.15	-21 26 49.5	1	1	-1.07±0.29	0.44±0.42
2	8	-88.2	-8.3	17 27 35.38	-21 27 17.3	...	...	-1.42 0.51	-0.04 0.74
3	9	-86.4	-6.4	17 27 35.51	-21 27 15.4	...	...	-0.92 0.60	-0.10 0.58
4	10	-84.7	-4.2	17 27 35.63	-21 27 13.2	4	...	-1.87 0.51	-0.48 0.38
5	12	-84.3	35.9	17 27 35.67	-21 26 33.1	5	(3)	0.20 0.47	2.58 0.25
6	10	-84.2	25.3	17 27 35.67	-21 26 43.7	3	2	0.09 0.25	1.13 0.54
7	8	-82.9	-2.8	17 27 35.77	-21 27 11.8	...	...	-1.28 0.79	0.70 0.54
8	10	-82.4	33.2	17 27 35.80	-21 26 35.8	...	...	-0.21 0.31	0.21 0.63
9	11	-82.0	29.9	17 27 35.83	-21 26 39.1	...	20	1.76 0.74	0.45 0.40
10	5	-81.9	46.6	17 27 35.83	-21 26 22.4	6	...	0.61 2.56	-2.09 3.18
11	8	-81.6	-2.5	17 27 35.86	-21 27 11.5	...	...	-0.09 0.96	0.02 0.45
12	10	-80.2	23.2	17 27 35.95	-21 26 45.8	9	...	-0.31 0.29	1.58 0.60
13	10	-80.2	-1.6	17 27 35.95	-21 27 10.6	8	4	-0.63 0.53	1.02 0.49
14	8	-79.5	24.3	17 27 36.00	-21 26 44.7	...	(21)	0.15 0.95	2.61 1.68
15	8	-79.2	20.2	17 27 36.02	-21 26 48.8	...	...	-0.86 0.12	0.93 0.66
16	10	-79.2	29.3	17 27 36.02	-21 26 39.7	10	...	-1.04 0.82	0.49 0.25
17	9	-79.1	-0.2	17 27 36.03	-21 27 9.2	...	5	-0.94 0.35	0.80 0.38
18	11	-78.4	34.7	17 27 36.08	-21 26 34.3	11	7	0.54 0.28	1.46 0.38
19	11	-76.9	36.4	17 27 36.19	-21 26 32.6	...	8	-1.73 0.51	-0.42 0.65
20	9	-76.9	45.6	17 27 36.19	-21 26 23.4	12	(22)	-0.29 0.21	1.20 0.18
21	7	-76.8	0.0	17 27 36.20	-21 27 9.0	...	...	-0.46 0.22	-0.61 0.63
22	11	-75.8	24.2	17 27 36.27	-21 26 44.8	15	...	-0.63 0.51	-0.55 1.27
23	10	-74.7	40.0	17 27 36.35	-21 26 29.0	17	...	-3.75 0.40	-0.50 0.15
24	9	-74.4	21.8	17 27 36.37	-21 26 47.2	18	9	-0.94 0.11	1.13 0.27
25	12	-74.1	42.9	17 27 36.39	-21 26 26.1	19	...	-3.65 0.76	1.31 0.16
26	9	-73.5	26.6	17 27 36.44	-21 26 42.4	(20)	23	0.71 1.03	0.81 0.53
27	10	-71.8	46.1	17 27 36.56	-21 26 22.9	21	...	-1.00 0.15	1.09 0.50
28	11	-70.8	43.4	17 27 36.63	-21 26 25.6	23	(24)	-0.25 0.49	1.88 0.46
29	11	-69.2	40.2	17 27 36.74	-21 26 28.8	25	...	-0.19 0.46	0.74 0.60
30	11	-67.7	46.8	17 27 36.85	-21 26 22.2	...	(25)	-2.85 0.44	1.81 0.26
31	10	-67.1	49.8	17 27 36.90	-21 26 19.2	(27)	...	-1.83 0.38	1.11 0.32
32	6	-65.5	44.0	17 27 37.01	-21 26 25.0	...	...	-1.18 0.28	0.42 0.38
33	9	-64.8	46.6	17 27 37.06	-21 26 22.4	...	...	-1.43 0.45	3.67 0.71
34	8	-64.5	48.7	17 27 37.08	-21 26 20.3	...	26	-1.56 0.61	2.00 1.18
35	7	-50.1	-16.1	17 27 38.11	-21 27 25.1	30	...	-2.28 0.59	1.64 1.06
36	6	-46.2	83.0	17 27 38.39	-21 25 46.0	...	...	2.11 0.99	0.47 0.81
37	6	-44.3	83.1	17 27 38.53	-21 25 45.9	31	...	0.05 1.59	1.56 0.60
38	10	-32.9	6.9	17 27 39.34	-21 27 2.1	34	...	0.72 0.64	-0.07 0.22
39	9	-30.6	8.3	17 27 39.51	-21 27 0.7	35	...	-1.33 0.29	0.12 0.32
40	6	-29.5	9.5	17 27 39.59	-21 26 59.5	...	...	-1.13 0.80	0.30 0.56
41	9	-27.3	12.9	17 27 39.74	-21 26 56.1	37	11	-0.87 0.39	0.38 0.36
42	4	-26.1	4.6	17 27 39.83	-21 27 4.4	38	...	-2.19 0.75	1.45 1.52
43	5	-23.3	3.3	17 27 40.03	-21 27 5.7	39	...	-3.84 3.01	1.41 1.68
44	10	-21.4	4.7	17 27 40.17	-21 27 4.3	40	12	-1.61 0.35	-0.17 0.39
45	10	-14.4	10.4	17 27 40.67	-21 26 58.6	...	...	1.56 0.88	-1.77 0.60
46	10	-13.1	9.5	17 27 40.76	-21 26 59.5	43	13	0.11 0.78	0.32 0.27
47	9	-3.8	83.9	17 27 41.43	-21 25 45.1	46	15	-0.95 0.20	-0.91 0.56
48	10	35.0	74.9	17 27 44.20	-21 25 54.1	56	18	-0.18 0.40	1.34 0.32
49	10	39.9	66.1	17 27 44.56	-21 26 2.9	59	19	-0.42 0.27	0.06 0.14
50	10	51.4	-24.0	17 27 45.38	-21 27 33.0	64	...	0.32 0.61	-1.24 0.50

brightening rapidly. In window No. 7 (Fig. 11) knot 35 appears to be brightening. Proximity to a rather bright star makes it difficult to establish its earliest evolutionary history. (Figure 12) shows that the single long filament in window No. 8 does not exhibit any obvious evolution over the period 1942–1989. Finally window No. 9 (see Fig. 13) contains an isolated old knot (No. 1).

The observations discussed above appear to show that new knots occur mainly in the northern part of the remnant along the outer edge of the nebulosity (which is coincident with the edge of the radio and X-ray remnant). A similar conclusion was previously reached by van den Bergh & Kamper (1977) on the basis of the more limited data that were available at that time. In the central part of the remnant new knots are presently only appearing to the south of already existing ones. The geometry of the regions where new knots are forming can be understood in terms of the model of Bandiera (1987, 1988) in which a blast wave interacts with a sheet of material that formed when the progenitor's wind was interacting with the interstellar medium.

Details of the geometry of the evolution, as well as a more extensive discussion of its relation to theoretical models, will be given in Bandiera (1991).

More quantitative information on the positions and brightness variations of 50 knots in Kepler's SNR will be presented in the next section.

### 3.2. The Catalog of Knots

A catalog of proper motions for a set of 19 bright knots in Kepler's supernova remnant has previously been presented by van den Bergh & Kamper (1977). In that paper the positions of individual knots were determined manually, and special procedures were employed to avoid various kinds of bias. More recently D'Odorico et al (1986) have presented a catalog of positions and fluxes for 64 knots in Kepler's SNR. This catalog is based on high-quality CCD images and therefore knots fainter than those observed by van den Bergh & Kamper (1977) can be detected. However, it is based on only a single

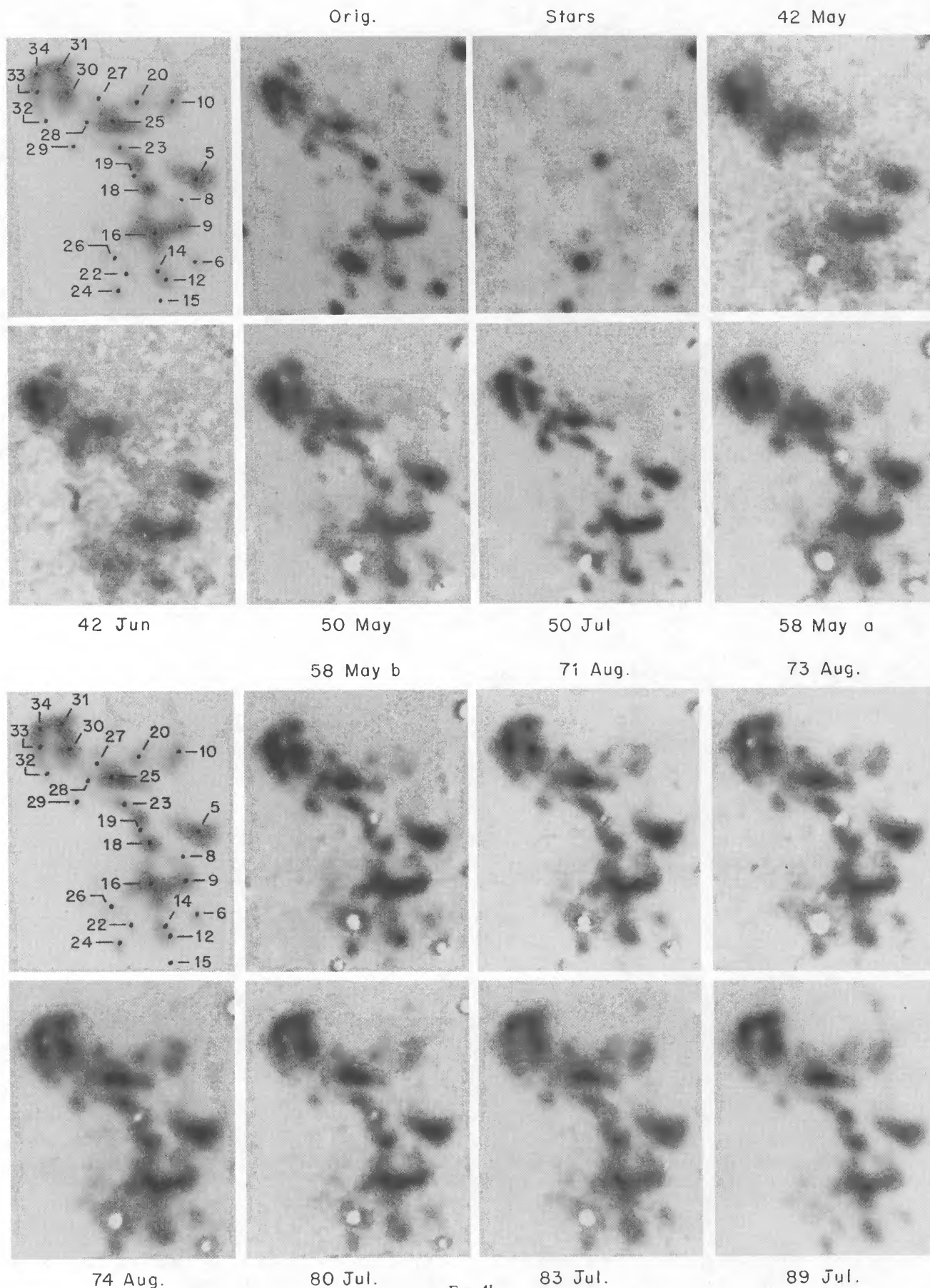


FIG. 4b

FIG. 4.—(a-b) Evolution of bright knots in window No. 1

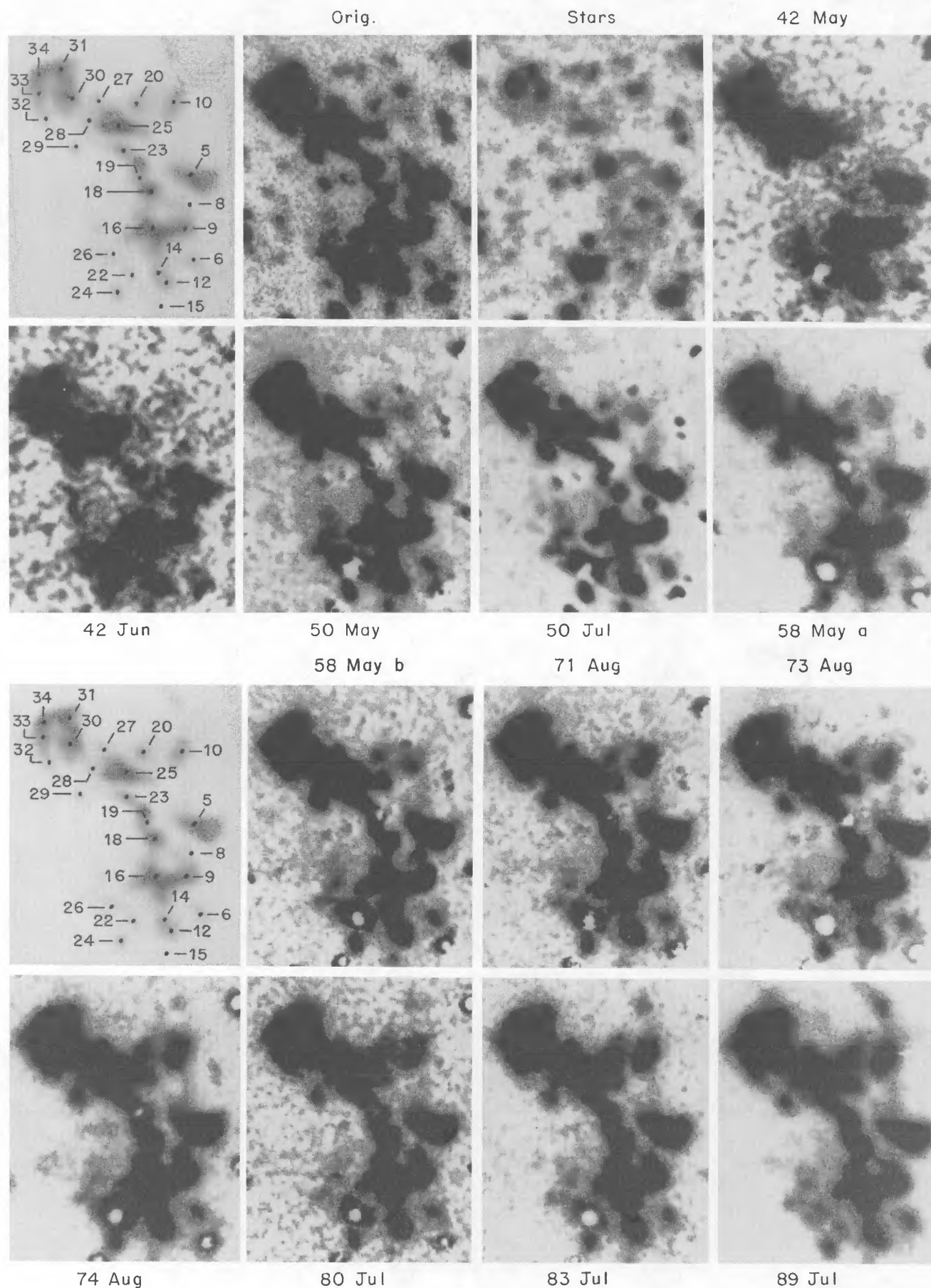


FIG. 5b

FIG. 5.—(a-b) Evolution of faint knots in window No. 1

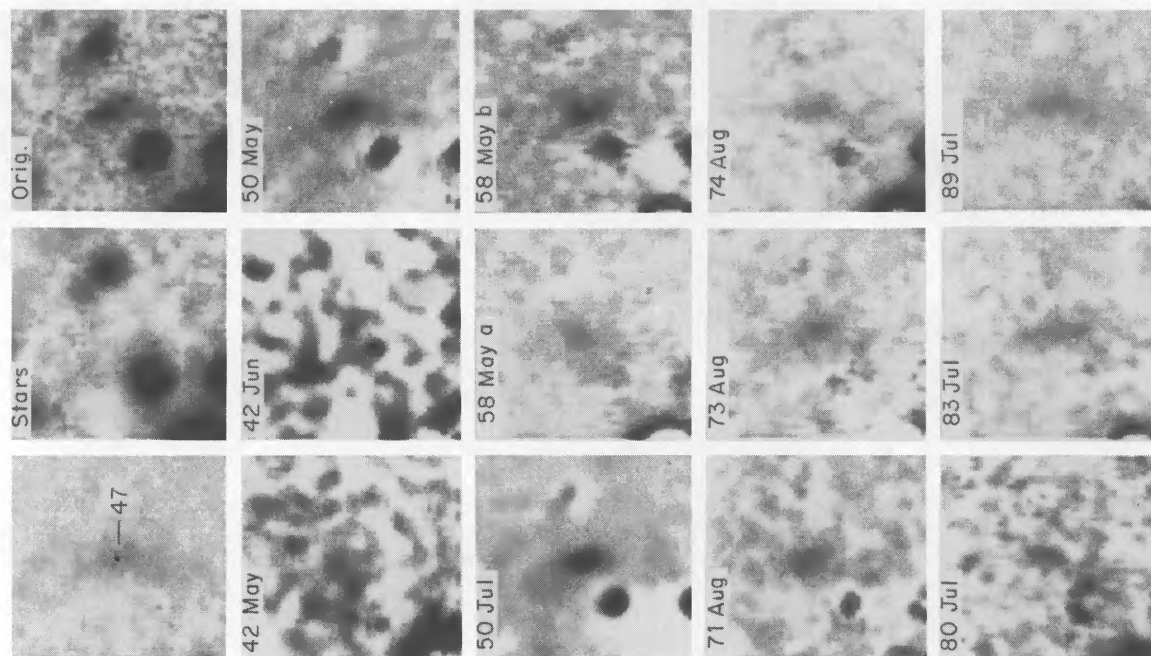


FIG. 7.—Evolution of knots in window No. 3

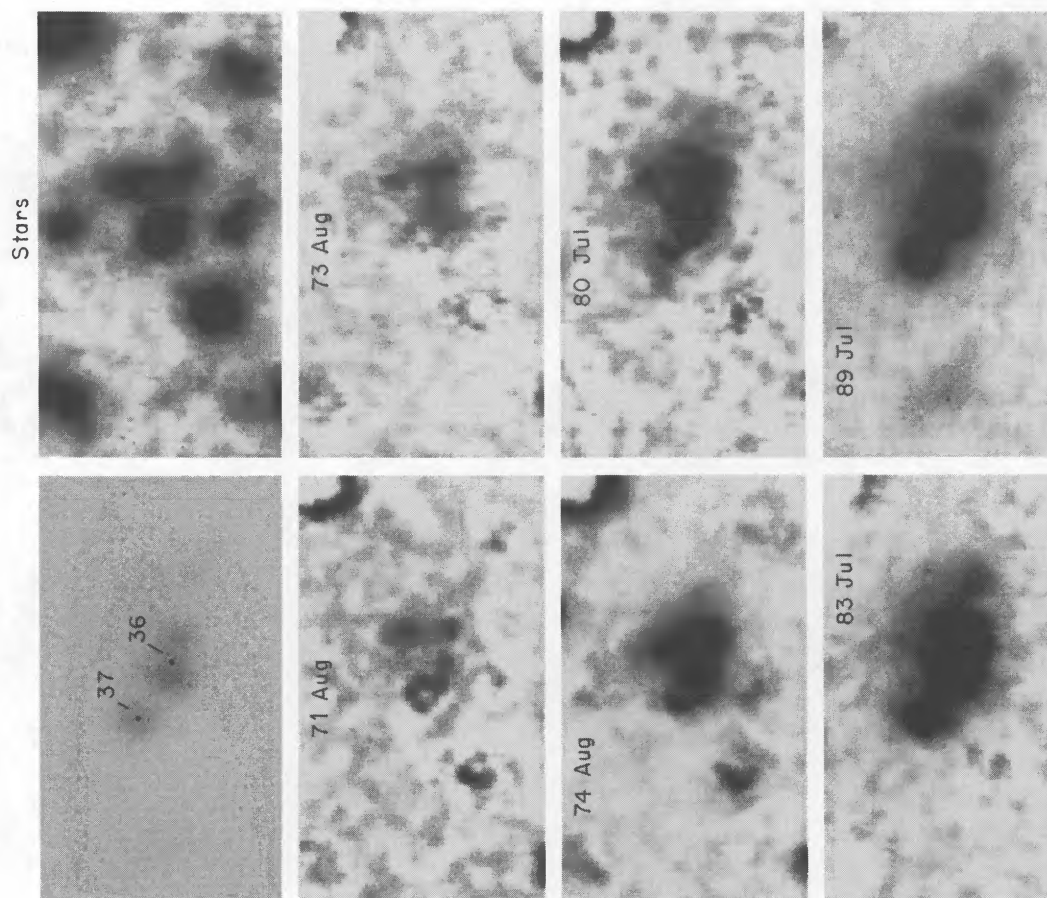


FIG. 6.—Evolution of knots in window No. 2

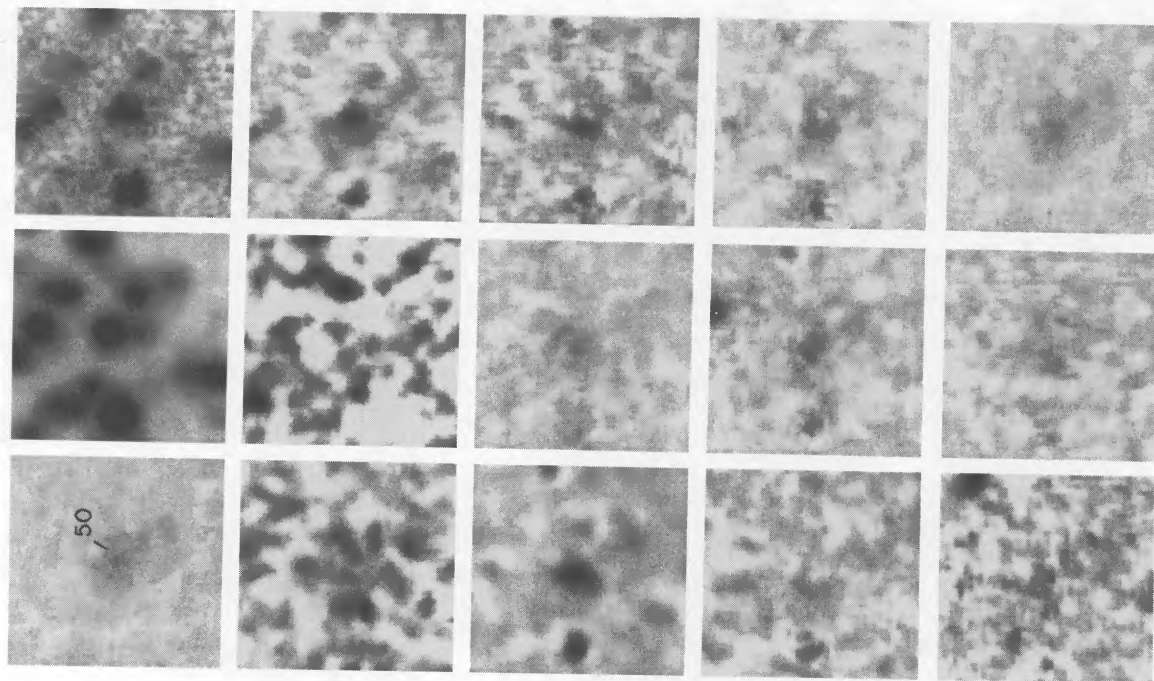


FIG. 9.—Evolution of knots in window No. 5

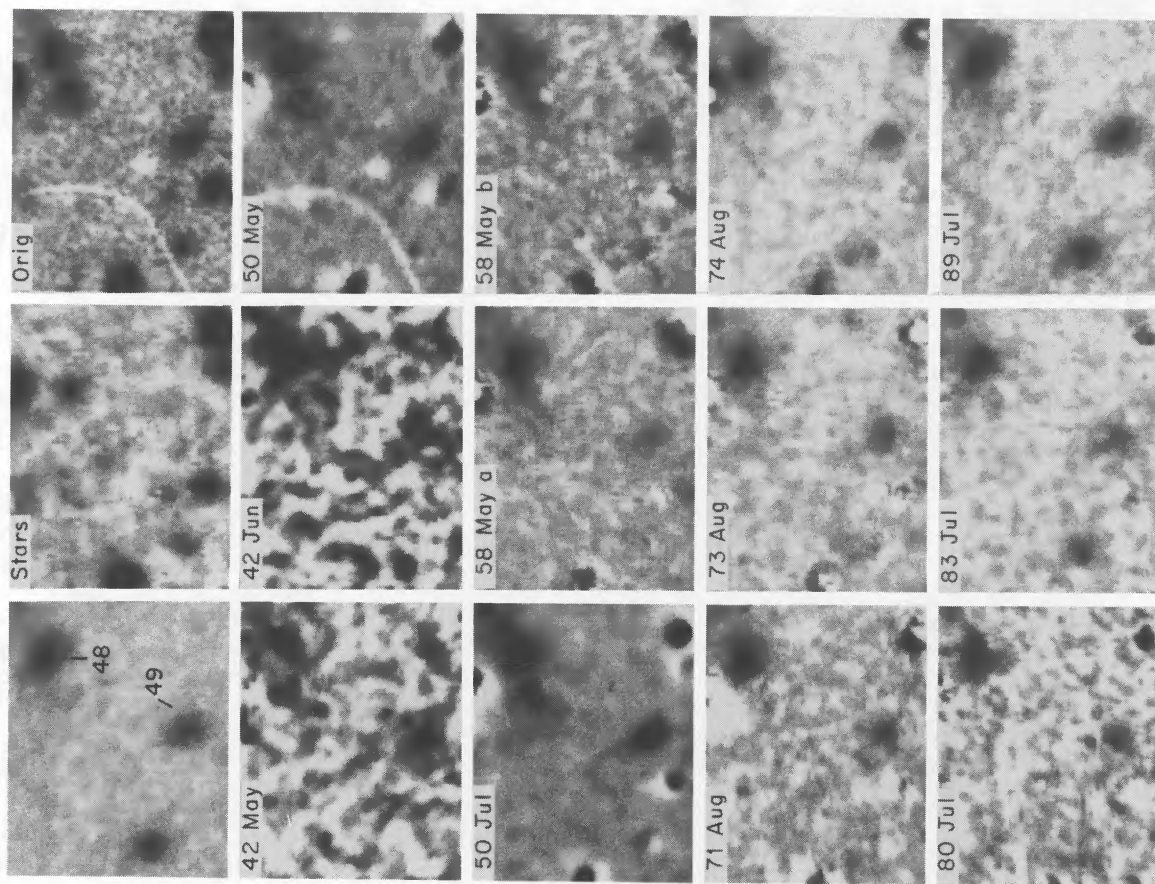


FIG. 8.—Evolution of knots in window No. 4

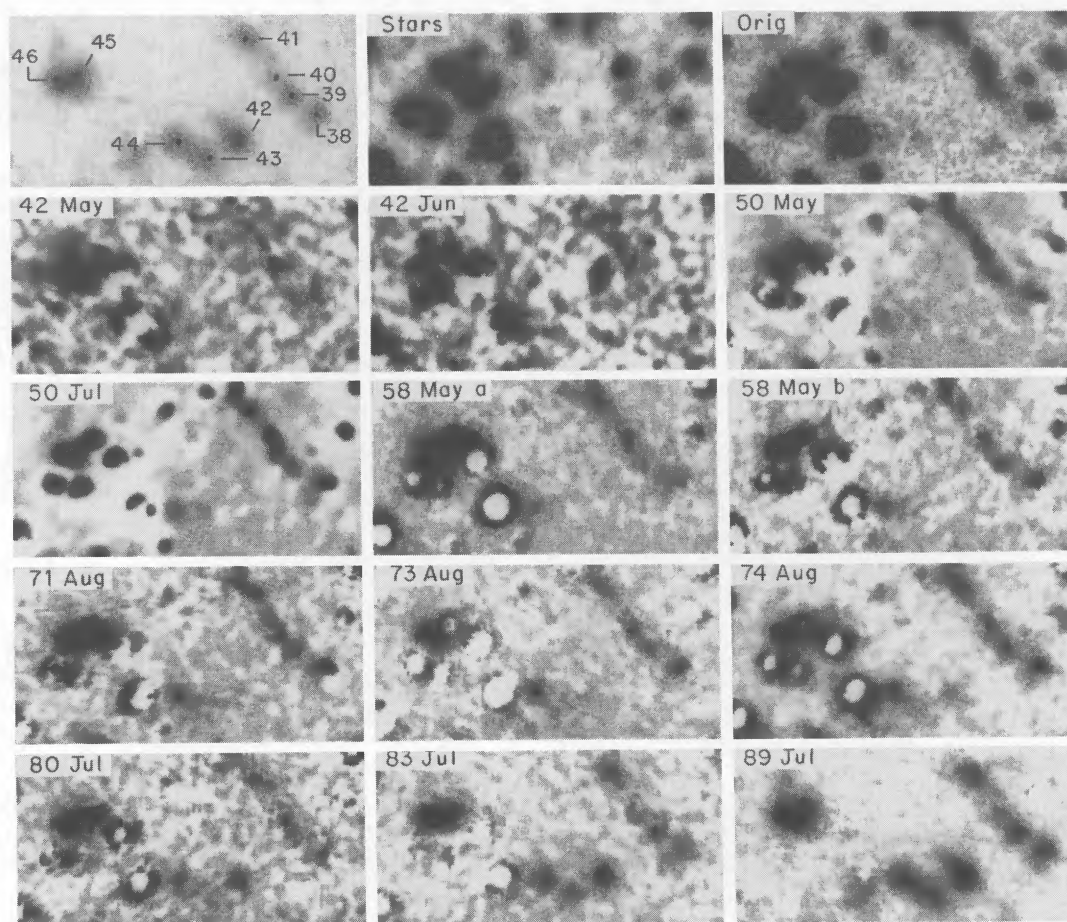


FIG. 10.—Evolution of knots in window No. 6

observation of each knot. For this reason in crowded regions identification of individual components might be ambiguous. We have preferred to use a safer procedure in which a knot is only regarded as real if it can be identified on multiple images.

Our catalog, which is presented in Table 3, was prepared from an automated search of images that had been cleaned by prior subtraction of stellar images. As a result the number of knots found was twice that studied by van den Bergh & Kamper (1977) on a set of plates including some used in the present study. In our investigation, the absence of stellar contamination in individual images made it much easier to separate compact groups of knots into individual components and to determine the fluxes of individual knots. The catalog given in Table 3 was compiled using the INVENTORY routine in each of the nine windows shown in Figure 3. In each of these windows different search threshold, background fitting, and limiting separation parameters were employed. However, the same set of search parameters was used for all plates of a given window. Only those knots which were selected independently by INVENTORY on a number of different frames were retained in the final analysis. Moreover, except for the CCD image which is very clean, most windows contain some poorly subtracted bright stars that were detected by the routine for automatic search; they have been subsequently removed by visual inspection. On average, each knot was detected on nine of the 12 available frames. The positions

derived for the same knot may differ slightly from plate to plate. In some ambiguous cases a human decision was needed. However, we are confident that such subjective decisions had only a minor influence on the results presented below.

Since the relative positions of knots on different plates are very well determined they can, by a least-squares procedure, be used to derive the proper motions of individual features listed in Table 3. In making these solutions it was assumed that the knots suffer no accelerations. Furthermore all data points were given equal weight. The absolute positions of knots were based on the absolute reference frame employed by D'Odorico et al. (1986), by minimizing the displacements between corresponding knots. Using this procedure we expect to have attained an accuracy of  $\sim 0''.1$ . Thirty of the 50 knots listed in Table 3 coincide within  $1''$  with knots observed by D'Odorico et al. (1986), while 16 of them correspond with the same accuracy to knots listed in the van den Bergh & Kamper (1977) catalog. Cross references between these catalogs are listed in Table 3. Some further correspondences, even if not so close, are likely and we have added them in Table 3 in parentheses. When making comparisons with other catalogs, we always corrected the positions of knots for proper motion.

Table 3 is organized as follows. Column (1) lists all knots in order of increasing R.A. column (2) gives the number of frames on which each knot was measured, columns (3) and (4) give the 1970 positions, measured in arcseconds, of knots relative to

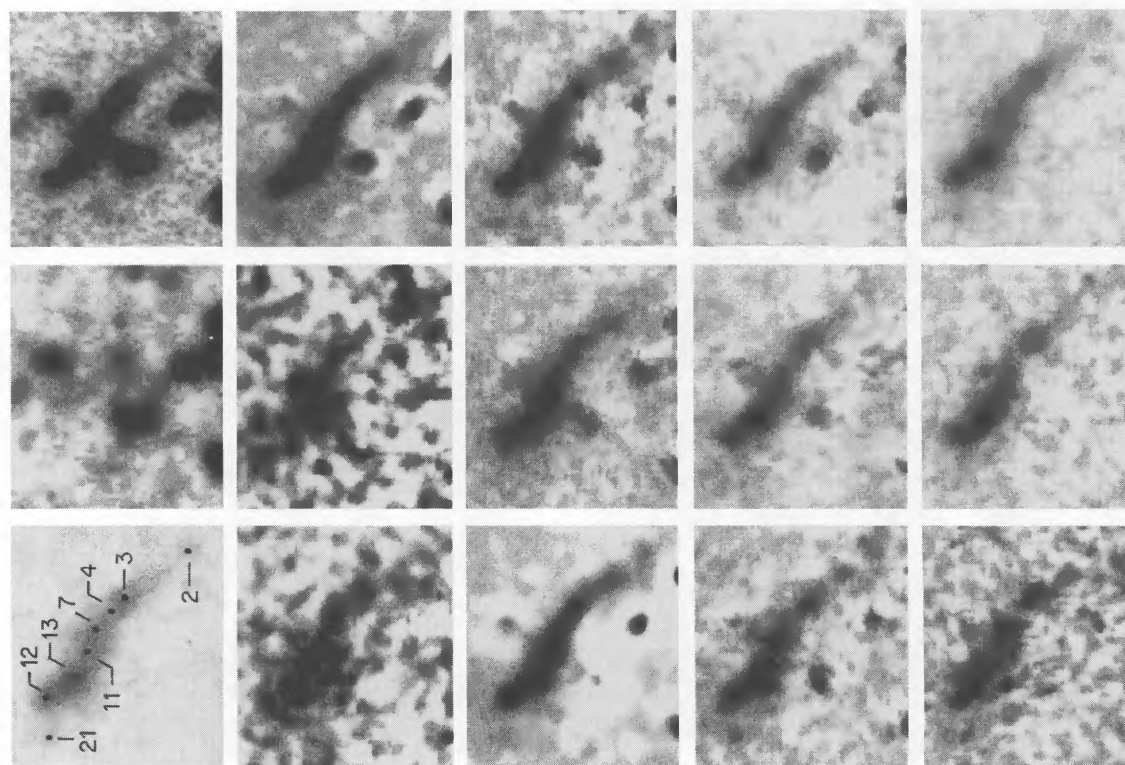


FIG. 12.—Evolution of knots in window No. 8

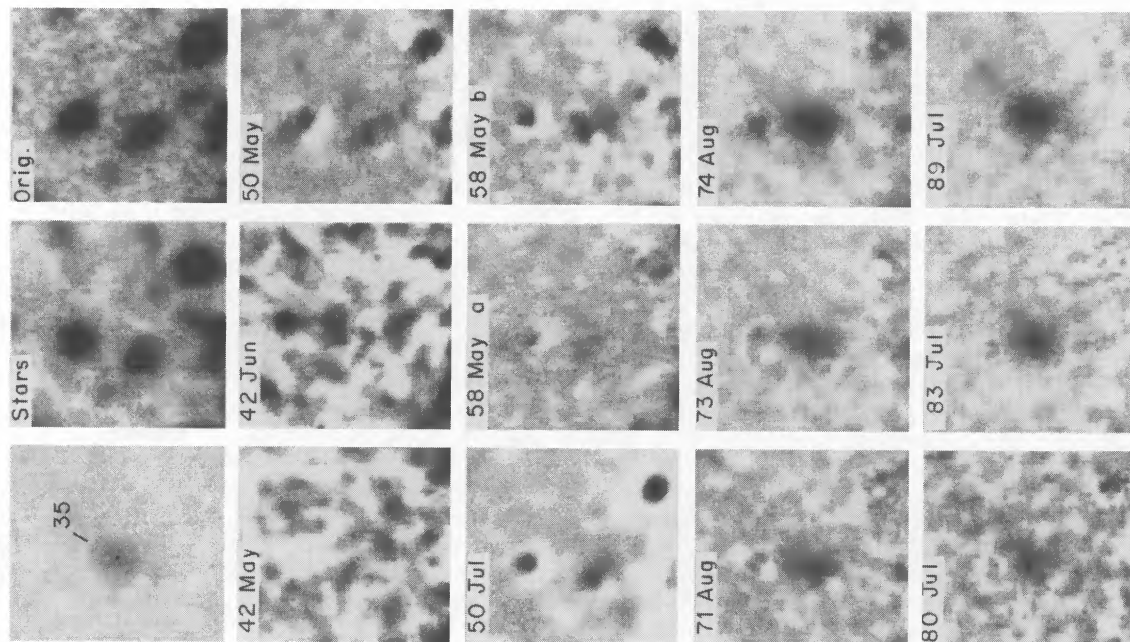


FIG. 11.—Evolution of knots in window No. 7

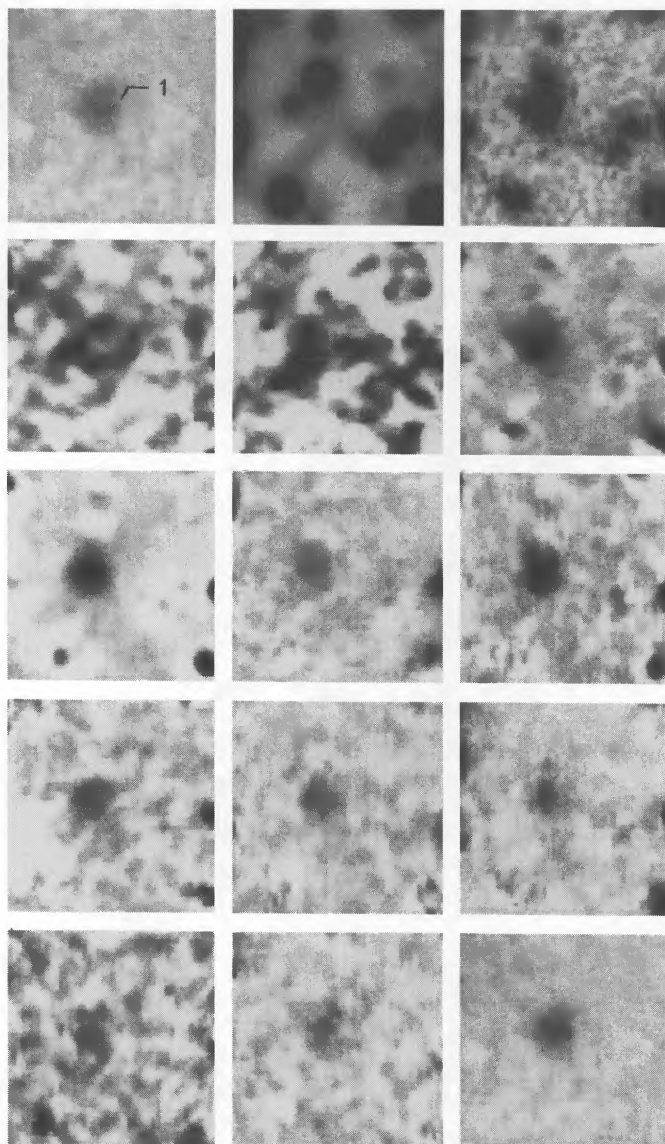


FIG. 13.—Evolution of knots in window No. 9

the center of the radio remnant at  $\alpha(1950) = 17^{\text{h}}27^{\text{m}}41^{\text{s}}.7$ ,  $\delta(1950) = -21^{\circ}27'09''$  (Matsui et al. 1984). The positive  $x$  and  $y$  axes point toward the east and north, respectively. Columns (5) and (6) list the coordinates of individual knots for Epoch 1950, extrapolated again to 1970 for knots proper motions. Columns (7) and (8) give cross references to the knot designations of D'Odorico et al. (1986; labeled "DBDF") and van den Bergh & Kamper (1977; labeled "vdBK"), respectively. Finally, columns (9) and (10) give the proper motions  $\mu_x$  and  $\mu_y$  with their respective errors, in arcseconds per century.

### 3.3. Expansion of the Nebula

Figure 14 shows the positions of individual knots. Arrows indicate the 400 yr proper motions, i.e., the motions during a period comparable to the age of the remnant. A least-squares solution for a general spherical expansion of the nebula, together with a translation of the center of expansion, yields  $\langle \mu_x \rangle = -0''.623 \pm 0''.045 \text{ century}^{-1}$  and  $\langle \mu_y \rangle = 0''.484 \pm 0''.049$

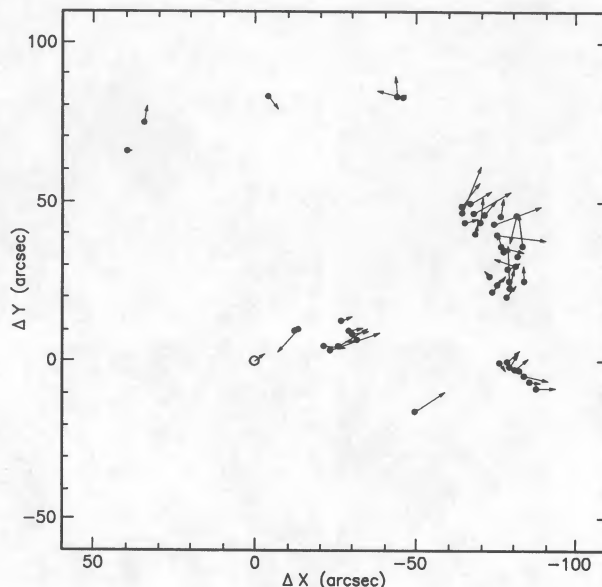


FIG. 14.—Positions and 400 yr proper motions of knots in Kepler's SNR. The open circle shows the position of the radio center of the remnant. The arrow attached to this circle shows the 400 yr proper motion of the center of expansion of the optical remnant.

century $^{-1}$  and an expansion time scale of  $32,000 \pm 12,000$  yr. The present results are seen to be consistent with those of van den Bergh & Kamper but have significantly higher weight. Assuming a mean distance of 1.4 kpc for the foreground field stars and a distance of 4.5 kpc for Kepler's supernova (see § 3.5), and correcting for Galactic rotation (see Bandiera 1987, based on Clemens 1985), one obtains velocities of  $117 \pm 10 \text{ km s}^{-1}$  and  $105 \pm 11 \text{ km s}^{-1}$  toward the W and N, respectively, and an expansion velocity  $v_{\text{exp}} = 67 \pm 26 \text{ km s}^{-1}$ . We are confident that the uncertainties estimated by the least-squares method are reliable, and that the derived translation is not just a statistical artifact. One could argue that the determination of such a translation is rather uncertain, because most of the knots are located on the same side of the remnant. However, the presence of several knots in the central regions allows our procedure to distinguish between expansion and translation rather well. Independent evidence in favor of a common translation comes from radial velocities of knots (van den Bergh & Kamper 1977). Which are consistent with no expansion, and indicate a conspicuous common velocity. We note in particular that many of the radial velocities of knots are measured close to the edge of the shell and cannot therefore be ascribed to expansion. When corrected for Galactic rotation it turns out to be  $-229 \pm 13 \text{ km s}^{-1}$  (Bandiera 1987). By combining radial and tangential velocities we find that the center of expansion has a very high space velocity of  $278 \pm 12 \text{ km s}^{-1}$ . The velocity of the center of expansion is directed away from the Galactic plane from which it is receding at a velocity of  $127 \pm 10 \text{ km s}^{-1}$ . Since we attempted a purely kinematical fit, the optical knots need not to be a representative sampling of the entire circumstellar mass. All that is required is that they adequately cover the area occupied by the remnant. The fact that they cover only about half of that area implies that motions more complex than a combination of translation and expansion could not be adequately described.

The observed motion of the center of expansion of the remnant is consistent with either a progenitor that belonged to

Population II, or with a massive progenitor that escaped from the Galactic plane as a high-velocity star (Bandiera 1987)  $\sim 4.0$  million years ago. The low expansion velocity of the remnant is consistent with the idea that it consists of circumstellar material that was excited by shock waves produced during the supernova explosion. The measured expansion velocity could be partly due to the original wind and partly due to the impact with the shock; a lower limit to the density contrast in knots is therefore  $\sim (v_{\text{sh}}/v_{\text{exp}}) \sim 40$  (for  $v_{\text{sh}} \simeq 2700 \text{ km s}^{-1}$ ; Dickel et al. 1988).

### 3.4. Light Curves of Individual Knots

While extracting a list of objects from a frame, the INVENTORY routine also estimates the intensities of all objects. Since the photographic plates available for the present investigation were not calibrated it was impossible to derive absolute photometry for individual knots directly. We were, however, able to extract *approximate* photometric information by direct comparison of the intensities of corresponding knots in different images. Such comparisons have been applied between plates adjacent in time, since in these cases the number of common knots is largest and the brightness evolution is expected to be small. However, since most knots are fading, a bias is intrinsic in this method. Because of it intensity distributions tend to get steeper at later times. We corrected for this effect by also assuming that the slope of the intensity distribution remained constant in time. Intensity estimates obtained by this procedure are believed to be accurate to  $\sim 10\%$  between plates that are adjacent in time, and to  $\sim 30\%$  for the others.

The knot fluxes given by D'Odorico et al. (1986) were used to fix the absolute intensity scale. Knots 10, 36, 37, 42, and 43 are found to be brightening rapidly, while knots 18, 20, and 31 are brightening more slowly. The knots 27, 30, 34, and 44 appear to be on a luminosity plateau, after having brightened during the early part of the present observing period. Knots 4, 5, 7, 47, and 48 are possibly beginning to fade, while knots 1, 11, 15, 28, 29, 33, and 50 are fading steadily. Within the accuracy of the present data knots 6, 16, 24, 25, 35, 39, 41, and 46 have remained approximately constant in luminosity over the last  $\sim 50$  yr. In no case did a knot first brighten and then fade during the last half century. In this respect the knots in Kepler's SNR are similar to the quasi-stationary flocculi in Cas A (van den Bergh & Kamper 1985), which were found to have lifetimes  $\geq 25$  yr, with only two cases of brightening (R36 and R37) and one possible case of fading (R38). A completely different behavior is exhibited by the fast-moving knots in Cas A. Some of these were found to have quite short lifetimes. The absolute intensities of individual knots (on a logarithmic scale, calibrated via D'Odorico et al. 1986), are listed in Table 4. In a subsequent paper we shall attempt to correlate excitation conditions in individual knots with phase in their light cycle.

### 3.5. Reddening, Distance, and Luminosity of SN 1604

In October of 1604 Mars, Jupiter and SN 1604 were located within a few degrees of each other in the sky (Baade 1943). This proximity facilitated intercomparison of the magnitudes and colors of these three objects. According to the data listed in Table 2 of Baade's paper, observers on 1604 October 9 ( $\Delta T = -8$  days), and 1604 October 10 ( $\Delta T = -7$  days) state that the color of the supernova resembled that of Mars, whereas two observers on 1604 October 15 ( $\Delta T = -2$  days) claim that the color of this object was similar to that of Jupiter.

According to Harris (1961)  $\langle B-V \rangle = 1.36$  for Mars and  $\langle B-V \rangle = 0.83$  for Jupiter.

These color estimates provide information on the supernova type and/or on its reddening. From a compilation of all published UBV photometry of supernovae Younger & van den Bergh (1985) find that both SNIa and SNII typically have  $(B-V)_0 \simeq 0.0$  (with an uncertainty of  $\sim 0.1$  mag) at maximum light ( $\Delta T = 0$  days). It therefore follows that the reddening of Kepler's supernova, if it belonged to one of these types, probably lies in the range  $0.8 < E_{B-V} < 1.4$ , corresponding to  $2.5 < A_V < 4.3$  mag. Our evaluation of the uncertainty of the reddening of SN 1604, i.e.,  $E_{B-V} = 1.10 \pm 0.26$ , is less optimistic than that of Pskovskii (1978), who adopts  $E_{B-V} = 1.27 \pm 0.04$ . However, the latter determination includes both unrealistically blue intrinsic colors for  $\Delta T < 0$  and a value  $B-V = 0.6$ : for the supernova on 1604 October 9, when Altobelli in Verona describes it as resembling "a half-ripe orange"!

Our absorption value ( $A_V = 3.4 \pm 0.9$ ) is consistent with those which Danziger & Goss (1980) and Dennefeld (1982) obtain from measurements of the Balmer decrement in the optical remnant of Kepler's supernova. Note, however, that Leibowitz & Danziger (1983) find knot-to-knot differences in Balmer decrements, that correspond to a range of up to 2 mag in the absorption values for different knots in Kepler's SNR. This could mean that the reddening is very patchy in Kepler's SNR field, so that no information on the supernova reddening can be inferred. Alternatively, part of the Balmer decrement could be intrinsic to the knots themselves, in which case an upper limit to the cosmic reddening should be derived from the smallest Balmer decrement observed ( $A_V \lesssim 2.8$ , leading to  $E_{B-V} \lesssim 0.9$ ; Leibowitz & Danziger 1983). The latter hypothesis is consistent with the lower reddening estimated from the auroral [S II] lines (Dennefeld 1982).

A viable alternative is that SN 1604 was a type Ib supernova. At maximum light SNIb appear to be significantly redder (Uomoto & Kirschner 1985) than SNIa and SNII. As a result, the reddening of Kepler's SN might be as small as the foreground reddening,  $E_{B-V} \simeq 0.7 \pm 0.2$ , corresponding to  $A_V = 2.2 \pm 0.6$  mag, which van den Bergh & Kamper (1977) obtained from UBV photometry of field stars in the direction of this object. This would also be consistent with the upper limit based on the Balmer decrement and the estimate based on the auroral [S II] lines. A less stringent lower limit  $E_{B-V} \simeq 0.6$  is obtained from the 21 cm line absorption measurement by Hughes, Thompson, & Colvin (1971).

From a rediscussion of historical observations Clark & Stephenson (1977) find that SN 1604 had  $V(\text{max}) = -3.0$ . Other estimates are  $V(\text{max}) = -3.5$  (Pskovskii 1978) and  $V(\text{max}) = -2.5$  (Clark & Stephenson 1982). We shall therefore adopt  $V(\text{max}) = -3.0 \pm 0.5$ . From this it follows that  $V_0(\text{max}) = V(\text{max}) - A_V = -6.4 \pm 1.0$  if SN 1604 was of Types Ia or II; while, if it was of Type Ib, then  $V_0(\text{max}) = -5.2 \pm 0.8$ .

For the distance to Kepler's SNR we shall adopt the value  $D = 4.5 \pm 1.0$  derived by Bandiera (1987) from the kinematics of knots. This estimate is model dependent, since it assumes an interaction of the blast wave with a bow shock. Anyway the model used is consistent with the kinematic data, and some of its predictions (Bandiera 1987, 1988) have been recently verified (Bandiera 1991). Another kinematic distance estimate is presented by Braun (1987). It is based on a very different assumption, namely that the motions, apart from a random component, are radial, and that their barycenter follows

TABLE 4  
 $H\alpha + [N II]$  INTENSITIES OF KNOTS IN THE REMNANT OF KEPLER'S SUPERNOVA

	N.42MAY	42JUN	50MAY	50JUL	58MAY <sub>a</sub>	58MAY <sub>b</sub>	71AUG	73AUG	74AUG	80JUL	83JUL	89JUL
1	.....	-2.08	-2.38	-2.46	-2.36	-2.39	-2.50	-2.69	-2.64	-2.70	-2.76	-2.68
2	.....	.....	-3.07	-3.00	.....	-2.66	-2.73	.....	-3.06	-2.80	-3.28	-3.16
3	.....	.....	-2.63	-2.74	-2.38	-2.55	-2.65	-2.96	-2.81	-2.71	.....	-3.00
4	.....	.....	-2.40	-2.42	-2.32	-2.37	-2.39	-2.58	-2.51	-2.43	-2.70	-2.53
5	-1.28	-1.33	-1.08	-1.13	-1.12	-1.16	-1.11	-1.18	-1.18	-1.28	-1.29	-1.39
6	-1.61	.....	-2.16	-2.22	.....	-2.14	-2.04	-2.09	-2.12	-2.18	-2.14	-2.12
7	.....	.....	-2.27	.....	-2.22	.....	-2.32	-2.52	-2.42	-2.46	-2.67	-2.51
8	-1.64	.....	-2.01	-1.96	-1.95	-2.05	-2.02	-2.16	-2.05	-2.05	-2.14	.....
9	-1.30	-1.43	-1.52	-1.32	-1.46	-1.57	-1.51	-1.68	.....	-1.39	-1.53	-1.55
10	.....	.....	.....	.....	.....	.....	.....	-2.04	-1.99	-1.93	-1.80	-1.73
11	.....	.....	-2.20	-2.29	-2.12	-2.27	.....	-2.45	-2.38	.....	-2.52	-2.51
12	.....	-1.49	-1.60	-1.64	-1.57	-1.60	-1.73	-1.71	-1.74	-1.72	-1.84	.....
13	.....	.....	-2.18	-2.23	-2.18	-2.22	-2.18	-2.25	-2.32	-2.34	-2.33	-2.31
14	.....	-1.51	-1.60	-1.97	-1.79	-1.90	-1.84	.....	.....	.....	-1.74	-1.79
15	-1.63	.....	-2.28	-2.24	-2.32	-2.40	.....	.....	-2.57	.....	-2.71	-2.65
16	-1.31	-1.45	-1.32	-1.27	.....	-1.39	-1.28	-1.35	-1.29	-1.30	.....	-1.37
17	.....	.....	.....	-2.33	-2.25	-2.32	-2.26	-2.40	-2.49	-2.29	-2.45	-2.42
18	.....	-1.81	-1.77	-1.82	-1.74	-1.74	-1.63	-1.60	-1.51	-1.40	-1.37	-1.43
19	-1.62	-1.84	-2.02	-2.06	-1.82	-1.87	-1.78	-1.79	-1.79	-1.69	.....	-1.77
20	.....	.....	-2.36	-2.36	-2.10	-2.16	.....	-2.00	-2.00	-1.94	-1.86	-1.81
21	.....	.....	-2.84	-2.96	.....	-2.66	-2.64	.....	-3.03	.....	-3.26	-3.01
22	.....	-1.59	-2.15	-1.82	-1.99	-2.03	-2.07	-2.21	-1.92	-2.05	-2.20	-2.21
23	.....	.....	-1.68	-1.78	-1.56	-1.57	-1.61	-1.59	-1.50	-1.55	-1.71	-1.74
24	.....	.....	-1.90	-1.90	-1.88	-1.89	-1.90	-1.92	.....	-2.06	-1.98	-2.05
25	-1.33	-1.44	-1.30	-1.29	-1.35	-1.41	-1.25	-1.26	-1.26	-1.21	-1.22	-1.23
26	.....	.....	-1.92	-1.96	-1.88	.....	-2.05	-2.16	-1.99	-2.00	-2.13	-2.21
27	.....	.....	-2.04	-2.11	-1.84	-1.91	-1.79	-1.83	-1.84	-1.90	-1.87	-1.94
28	-1.32	-1.47	-1.62	-1.72	-1.59	-1.67	-1.78	-1.81	.....	-1.96	-1.88	-1.91
29	-1.30	-1.49	-1.69	-1.68	-1.76	-1.81	-1.90	-1.96	-1.90	.....	-2.03	-2.01
30	.....	-1.54	-1.49	-1.47	-1.37	-1.34	-1.33	-1.29	-1.23	-1.34	-1.39	-1.37
31	.....	-1.61	-1.71	-1.67	-1.63	-1.61	-1.46	-1.48	-1.44	.....	-1.25	-1.32
32	.....	.....	.....	-1.79	.....	.....	.....	-1.77	-1.80	-1.88	-1.89	-1.90
33	.....	-1.14	-1.09	-1.04	-1.03	-1.10	.....	-1.42	-1.42	-1.45	-1.48	.....
34	.....	.....	-1.90	.....	.....	-1.50	-1.28	-1.39	-1.40	-1.35	-1.29	-1.34
35	.....	.....	.....	.....	.....	-2.51	-2.44	-2.51	-2.36	-2.53	-2.45	-2.52
36	.....	.....	.....	.....	.....	.....	-2.42	-2.31	-2.04	-1.95	-1.82	-1.75
37	.....	.....	.....	.....	.....	.....	-2.49	-2.38	-2.10	-1.90	-1.87	-1.61
38	.....	.....	-2.41	-2.34	-2.42	-2.37	-2.15	-2.35	-2.21	-2.50	-2.57	-2.47
39	.....	.....	-2.47	-2.64	-2.42	-2.43	-2.42	-2.50	-2.38	.....	-2.43	-2.45
40	.....	.....	.....	-2.48	.....	.....	-2.40	-2.40	.....	-2.42	-2.74	-2.70
41	.....	.....	-2.38	-2.40	.....	-2.42	-2.31	-2.47	-2.28	-2.45	-2.47	-2.37
42	.....	.....	.....	.....	.....	.....	.....	.....	-2.62	-2.46	-2.16	-2.12
43	.....	.....	.....	.....	.....	.....	-2.82	-2.86	.....	-2.71	-2.51	-2.42
44	.....	.....	-2.74	-2.70	-2.36	-2.45	-2.34	-2.34	-2.26	-2.56	-2.37	-2.40
45	.....	.....	-2.21	-1.92	-2.05	-2.10	-2.19	-2.45	-2.30	-1.97	-2.36	-2.16
46	.....	.....	-1.96	-1.99	-1.90	-1.94	-1.88	-1.98	-2.02	-1.98	-2.02	-2.09
47	.....	.....	-2.48	-2.47	-2.44	-2.46	-2.49	-2.71	-2.71	-2.63	.....	-2.85
48	.....	.....	-2.23	-2.26	-2.10	-2.17	-2.12	-2.23	-2.22	-2.38	-2.44	-2.41
49	.....	.....	-2.39	-2.38	-2.51	-2.43	-2.50	-2.70	-2.66	-2.55	-2.72	-2.52
50	.....	.....	-2.49	-2.53	-2.44	-2.55	-2.79	-2.62	-2.75	-2.81	-2.98	-2.80

Galactic rotation. This assumption is, however, inconsistent with the results of van den Bergh & Kamper (1977), as well as with those presented in § 3.3 of this paper. Nonetheless the derived distance,  $4.1 \pm 0.9$  kpc, is not much different from that derived by Bandiera.

Distance estimates have also been derived from comparison with other SNRs, both in radio [5 kpc, by Caswell & Lerche 1979; 3 kpc and in X-rays ( $>5$  kpc, by Becker et al. 1980)]. Distance estimates based on the supernova  $V(\max)$  (e.g.,  $3.2 \pm 0.7$  kpc, by Danziger & Goss 1980; 4.2 kpc, by Strom 1988) are very uncertain because neither the supernova type nor the amount of reddening (as shown above) is well established.

By adopting  $D = 4.5 \pm 1.0$  kpc, we obtain  $(m - M)_0 = 13.3 \pm 0.5$ . The assumption that Kepler's supernova was a Type Ia or Type II and that it reached  $V_0(\max) = -6.4 \pm 0.9$  yields  $M_V(\max) = -19.7 \pm 1.0$ . The assumption that it was a Type Ib supernova with  $V_0(\max) = -5.2 \pm 0.8$  yields  $M_V(\max) = -18.5 \pm 0.9$ . Therefore the data discussed here cannot be used to determine whether SN 1604 was a supernova Type Ia (or a bright supernova of Type II), or a supernova of Type Ib. In general, indications about the nature of this object are rather

indirect, and even rather ambiguous. For instance, no neutron star has been detected inside the remnant. However, this result is still consistent with predictions of neutron stars cooling models (Tsuruta (1986). Moreover, the nebular remnant resembles that of Tycho's supernova in X-rays, but these two remnants are rather different in the optical. The nature of Kepler's SNR will be further discussed by Bandiera (1991).

It is a real pleasure to thank Allan Sandage and Leonard Searle for their efforts to locate Baade's plate of 1942 June 9. We also gratefully acknowledge the assistance of Michael Bolte and David Duncan with image processing and reduction of the CFH data. We are also indebted to Wes Fisher for digitizing some of the plates of Kepler's supernova remnant. One of us (S. v. d. B.) thanks the Directors of the Mount Wilson and Palomar Observatories for their kind hospitality during a large number of observing runs on the Palomar 5 m Hale telescope, and for permission to borrow old plates taken by Baade and Arp. Thanks are also due to F. Tribioli for his assistance with the UNIX version of MIDAS. Finally, we thank the referee (Virginia Tribble) for numerous helpful comments and suggestions.

## REFERENCES

- Baade, W. 1943, *ApJ*, 97, 119  
 Bandiera, R. 1987, *ApJ*, 319, 885  
 ———. 1988, in *Supernova Shells and Their Birth Events*, ed. W. Kundt (Berlin: Springer), p. 81  
 ———. 1991, in preparation  
 Becker, R. H., Boldt, E. A., Holt, S. S., Serlemitsos, P. J., & White, N. E. 1980, *AJ*, 237, L77  
 Bessel, M. S. 1983, *PASP*, 95, 480  
 Braun, R. 1987, *A&A*, 171, 233  
 Caswell, J. L. 1979, *MNRAS*, 187, 201  
 Clark, D. H., & Stephenson, F. R. 1977, *The Historical Supernovae* (Oxford: Pergamon Press), p. 191  
 ———. 1982, in *Supernovae: A Survey of Current Research*, ed. M. J. Rees & R. J. Stoneham (Dordrecht: Reidel), p. 355  
 Clemens, D. P. 1985, *ApJ*, 295, 422  
 Danziger, I. J., & Goss, W. M. 1980, *MNRAS*, 190, 49p  
 Dennefeld, M. 1982, *A&A*, 112, 215  
 Dickel, J. R., Sault, R., Arendt, R. G., Matsui, Y., & Korista, K. T. 1988, *ApJ*, 330, 254  
 D'Odorico, S., Bandiera, R., Danziger, J., & Focardi, P. 1986, *AJ*, 91, 1382  
 Fesen, R. A., Becker, R. H., Blair, W. P., & Long, K. S. 1989, *ApJ*, 338, L13  
 Harris, D. L. 1961, in *Planets and Satellites*, ed. G. P. Kuiper & B. M. Middlehurst (Chicago: University of Chicago Press), p. 272  
 Hughes, M. P., Thompson, A. R., & Colvin, R. S. 1971, *ApJS*, 23, 323  
 Leibowitz, E. M., & Danziger, I. J. 1983, *MNRAS*, 204, 273  
 Matsui, Y., Long, K. S., Dickel, J. R., & Greisen, E. W. 1984, *ApJ*, 287, 295  
 Pskovskii, Y. P. 1978, *Soviet Astr.*, 22, 420  
 Strom, R. G. 1988, *MNRAS*, 230, 331  
 Thuan, T. X., & Gunn, J. E. 1976, *PASP*, 88, 543  
 Tsuruta, S. 1986, *Comm. Ap.*, 11, 151  
 Uomoto, A., & Kirschner, R. P. 1985, *A&A*, 149, L7  
 van den Bergh, S., & Kamper, K. W. 1977, *ApJ*, 218, 617  
 ———. 1985, *ApJ*, 293, 537  
 van den Bergh, S., Marscher, A. P., & Terzian, Y. 1973, *ApJS*, 26, 19  
 West, R. M., & Kruszewski, A. 1982, *Irish AJ*, 15, 25  
 Younger, P. F., & van den Bergh, S. 1985, *A&A Suppl.*, 61, 365